Anal. Bioanal. Electrochem., Vol. 8, No. 1, 2016, 64-77

Analytical & Bioanalytical Electrochemistry

Full Paper

A Simple and Facile Electrochemical Route to Synthesis of Metal Hydroxides and Oxides Ultrafine Nanoparticles (M=La, Gd, Ni and Co)

RaminCheraghali[1,*] and Mustafa Aghazadeh[2]

[1]Chemistry Department, Saveh Branch, Islamic Azad University, Saveh, Iran
[2]Nuclear Science and Research Institute (NSTIR), Tehran, Iran

* Corresponding Author, Tel.: +98-21-82064289; Fax: +98-21-82064289
E-Mails: Ramincheraghali@yahoo.com, Mustafa.aghazadeh@gmail.com

Received: 15 December 2016 / Received in revised form: 26 January 2016 / Accepted: 27 January 2016 / Published online: 15 February 2016

Abstract- Ultrafine $M(OH)_n$ (M=La, Gd, Ni and Co) nanoparticles were electrochemically deposited from an additive–free $M(NO_3)_n$ (0.005 M) low-temperature bath on a steel substrate at the constant current density of 1 mA cm^{-2}. Heat–treatment of the prepared $M(OH)_n$ nanoparticles at 700°C led to formation of the oxide nanoparticles. The morphologies, crystal structures and compositions of the prepared products were determined by means of scanning (SEM) and transmission (TEM) electron microscopy as well as X-ray diffraction (XRD) and FT-IR spectroscopy. The results showed that the prepared $M(OH)_n$ samples are composed of ultrafine particles with the size of about 5 nm. After heat–treatment, the obtained products were well–crystallized phases of oxide nanoparticles with a size of around 10 nm. It was concluded that low-temperature cathodic electrodeposition offers a facile and feasible way for the preparation of ultrafine particles of metal oxides and hydroxides.

Keywords- Metal oxide, Metal Hydroxide, Nanoparticles, Cathodic electrodeposition, Heat-treatment

1. INTRODUCTION

Synthesis of metal hydroxides and oxides ($M(OH)_n$ and M_xO_n) at nanoscale with morphologies such as a particle, wire, tube and rod has recently found interesting research

area in nanotechnology. This is associated with their novel nanosize dependent physico-chemical properties, enhancing their effective surface area and maximizing their utilization in many different areas of technology.

In recent years, various physical and chemical techniques including chemical precipitation [1], sonochemical [2,3], sol–gel [4,5], solvothermal [6,7] and hydrothermal [8-10] methods have been employed for the synthesis of metal oxides and hydroxides at nano-scale. Compared to the above mentioned methods, electrodeposition appears to be a simple and facile method for the preparation of nanostructured oxides and hydroxides. This method has received more and more attention due to its inexpensive equipment, simple procedure and mild deposition conditions. Furthermore, easy control of the products morphology and composition is possible *via* bath conditions (e.g., temperature, concentration and pH), and applied electrochemical parameters (i.e., applied potential and current density). Thus, finding the optimum electrochemical conditions for preparation of nanostructured metal oxides and hydroxides, and specially one optimum electrodeposition condition for achieving ultrafine nanoparticles of $M(OH)_n$ and M_xO_n is interesting research area. Up to now, various nanostructures of metal oxides and hydroxides have been successfully prepared by cathodic electrodeposition from nitrate or chloride bath. For example, cathodic electrodeposition of yttrium compounds (i.e., $Y(OH)_3$ and Y_2O_3) has been extensively performed [11-14], and all these works are related to the preparation of thin films on the steel substrate. Recently, we applied cathodic electrodeposition for the preparation of nanostructured $Y(OH)_3$ and Y_2O_3 powders, and found that their various nanostructures including nanorods [15], nanospheres [16], nanocapsules [17], flaky-like [18] and brain-like [19] structures, and ultrafine nanoparticles [20] can be prepared by this facile method. About lanthanum, nanotubes [21,22], nanorods [23,24] and nanowires [25] of $La(OH)_3$ and La_2O_3 have been prepared by cathodic electrodeposition from nitrate bath using anodic alumina membrane as a template. It is also reported that $La(OH)_3$ and La_2O_3 nanospindles and nanorods can be obtained by galvanostatic deposition from DMSO-H_2O mixed solution [26]. Also, we found that cathodic electrodeposition from additive–free aqueous $La(NO_3)_3$ bath on steel substrate leads to formation of $La(OH)_3$ nanocapsules [27]. Heat–treatment of the obtained $La(OH)_3$nanocapsules resulted uniform La_2O_3 nanoplates [28]. Furthermore, La_2O_3 and $La(OH)_3$ nanorods [29] and nanowires [30] were prepared *via* cathodic electrodeposition without using any template. About gadolinium oxide and hydroxide, only a few reports are available in the literature [31-33]. In Ref. [31], thin films of Gd_2O_3 and organoceramic material has been prepared *via* cathodic electrodeposition from gadolinium hydroxide–poly(diallyldimethylammonium chloride) (PDDA) bath. It was also reported that rod-like and coral-like structures of Gd_2O_3 are achievable *via* cathodic electrodeposition [32,33]. The nanoporous films [34,35], nanoparticles [36], nanocapsules [37], and nano-whiskers [38] of $Ni(OH)_2$ and NiO have been also deposited by cathodic electrodeposition from chloride and

nitrate baths. Cathodic electrodeposition has been also applied as an attractive technique in the preparation of cobalt oxide and hydroxide nanoplates [39-45].

In this work, we focused on the optimum electrodeposition conditions for the preparation of ultrafine nanoparticles of metal hydroxides, and found that cathodic electrodeposition from metal nitrate bath at the mild conditions (i.e., low–temperature of 10^{o}C and low applied current density of 1 mA cm^{-2}) promotes the formation of very fine nanoparticles of $M(OH)_n$ (M=La, Gd, Ni and Co). Also, heat–treatment of the obtained nanoparticles at 700^{o}C in dry air atmosphere results the ultrafine oxide nanoparticles. Finally, based on the obtained results, we introduced low-temperature cathodic electrodeposition followed by heat-treatment as a general and facile method for the synthesis of ultrafine nanoparticles of metal hydroxides and oxides.

2. EXPERIMENTAL

Aqueous solutions (0.005 M) of $M(NO_3)_n.6H_2O$ (M=La, Gd, Ni and Co) were used as starting material in the electrodeposition experiments. The electrochemical cell included a stainless steel cathode (316 L, 100×50×0.5 mm) centered between the two parallel graphite counter electrodes. Prior to deposition, the steel substrates were given an galvanostatically electropolishing treatment at a current density of 20 A for 300s in a bath (80^{o}C) containing 50 vol.% phosphoric acid, 25 vol.% sulfuric acid and 25 vol.% deionized water. All of the electrodeposition experiments were performed galvanostatically at a current density of 1mA cm^{-2}. Bath temperature was fixed at 10^{o}C, and deposition time was 30 min. After deposition, the coatings were rinsed several times with distilled water and dried at RT for 24 h. The deposits were then scraped from the steel substrates and subjected to further analyses. For obtaining the oxide products, all the hydroxide samples were heat treated at the similar conditions. In fact, thermal annealing of all prepared hydroxide samples was performed in dry air flow between RT and 700^{o}C at a heating rate of 5 ^{o}C min^{-1}. The dwell time for all the samples was 3 h.

The crystallographic information was obtained by the powder X-ray diffraction (XRD) method using a Phillips PW-1800 diffractometer with Cu Kα radiation (λ=1.5406 Å) at a scanning rate of 1 degree/min. Chemical bonding information on metal–oxygen, metal–anions, and hydroxyl were studied with Fourier transform infrared spectroscopy (FTIR, Bruker Vector 22) using a potassium bromide (KBr) pellet technique. Each FTIR spectrum was collected after 20 scans at a resolution of 4 cm^{-1} from 400 to 4000 cm^{-1}. The weight percentages of carbon, hydrogen and nitrogen (CHN) in the prepared samples were measured in an ElementarVario ELIII analyzer. The surface morphologies were observed using a scanning electron microscope (SEM, LEO 1455 VP, Oxford, UK, operating voltage 15 kV) by mounting a small amount of prepared hydroxide powders on a conducting carbon tape and sputter coating with Pt to improve the conductivity. Transmission electron microscopy

(TEM) images were taken on a Phillips EM 2085 transmission electron microscope under a working voltage of 100 kV.

3. RESULTS AND DISCUSSION

Formation of the metal hydroxidedeposits (metal=La, Gd, Ni and Co) on the cathode surface can be explained on the basis of an electrochemical−chemical (EC) mechanism [46-49]; as schematically shown in Fig. 1.

1. Electrochemical step (base electrogeneration):

$$O_2 + 2H_2O + 4e^- \rightarrow 4OH^- \quad E^o = 0.26\ V \quad vs.\ Ag/AgCl \qquad (1\text{-}1)$$

$$2H_2O + 2e^- \rightarrow H_2 + 2OH^- \quad E^o = -1.08\ V \quad vs.\ Ag/AgCl \qquad (1\text{-}2)$$

$$NO_3^- + H_2O + 2e^- \rightarrow NO_2^- + 2OH^- \quad E^o = -0.21\ V \quad vs.\ Ag/AgCl \qquad (1\text{-}3)$$

2. Chemical step (deposit formation):

$$M^{n+}(aq) + (n\text{-}x)OH^-(aq) + y\ H_2O \rightarrow [M(OH)_n.yH_2O]\downarrow \qquad (2)$$

$$M^{n+}(aq) + (n\text{-}x)OH^-(aq) + x\ NO_3^- + y\ H_2O \rightarrow [M(OH)_{(n\text{-}x)}(NO_3)_x\ .yH_2O]\downarrow \qquad (3)$$

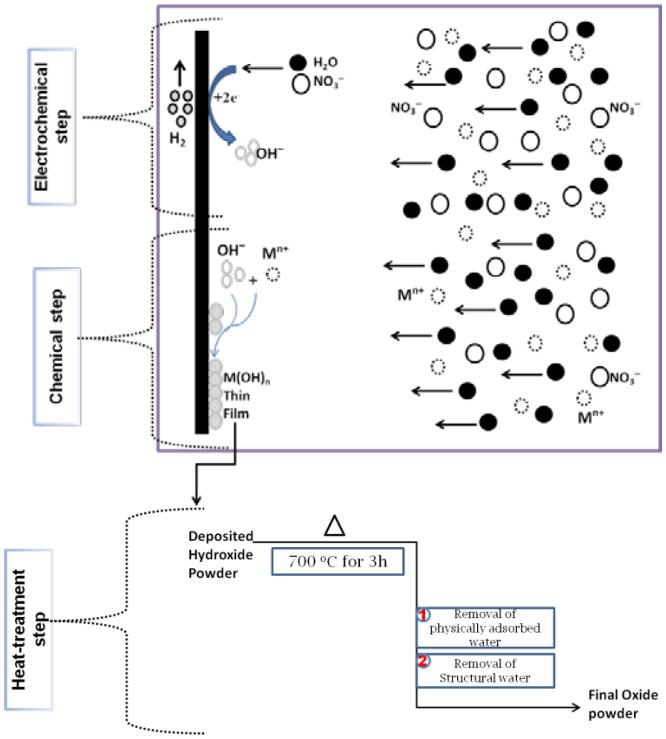

Fig. 1. A schematic view of hydroxide and oxide formation via cathodic electrodeposition-heat treatment

The hydroxyl ions are generated electrochemically by reduction of oxygen or water (Eqs. (1-1) and (1-2)). In baths containing nitrate anions, a reduction of these anions may participate to the generation of OH^- (Eq. (1-3)). Notably, electrogeneration of base *via* reduction of nitrate ions depends on the applied current or voltage in the deposition experiments [46]. The electrochemical step lead to a local increase of the OH^- concentration on the cathode surface and by increasing of pH to the required conditions in the reaction (2 and/or 3), so the chemical step is started and M^{n+} ions are sequentially deposited on the cathode surface in hydroxide form (Eqs. (2 and 3)) [48,49]. Finally, the prepared hydroxide powder is converted to the oxide product by heat-treatment at 700°C for 3h as schematically shown in Fig. 1.

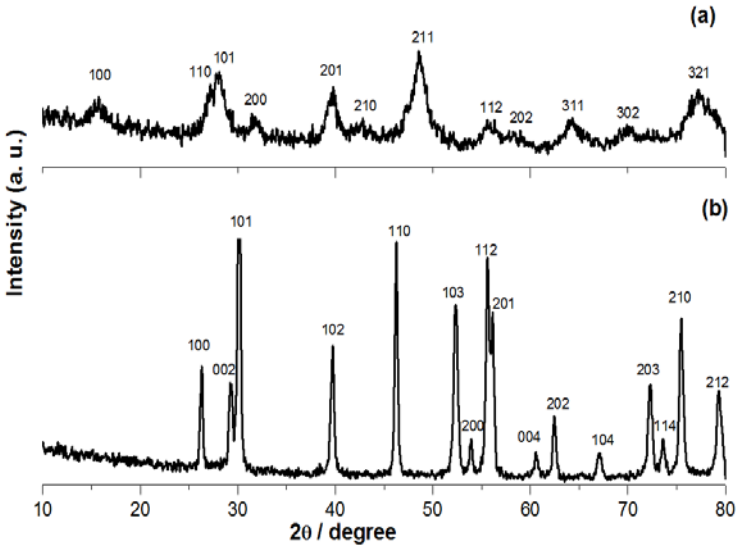

Fig. 2. XRD patterns of the prepared (a) $La(OH)_3$ and (b) La_2O_3 nanoparticles

Fig. 2a can be indexed as the hexagonal phase of $La(OH)_3$ with lattice constants *a*=6.528 Å and *c*=3.858 Å, which are completely consistent with the values in the standard card (*P63/m* (176), JCPDS 41-4019). The broadening of these diffraction peaks may indicates that the crystal size of $La(OH)_3$ particles is fine. The XRD pattern of the heat-treated sample at 700 °C (Fig. 2b) is easily assigned to a pure hexagonal phase (*P3m1* (164), JCPDS 05-0602) of La_2O_3 with lattice constants *a*=3.397 Å and *c*=6.129 Å. It should be noted that the width of peaks becomes narrow, which indicates that the grain size of oxide sample may be increased. The XRD patterns of nickel hydroxide compounds before and after heat treatment are shown in Fig. 3.

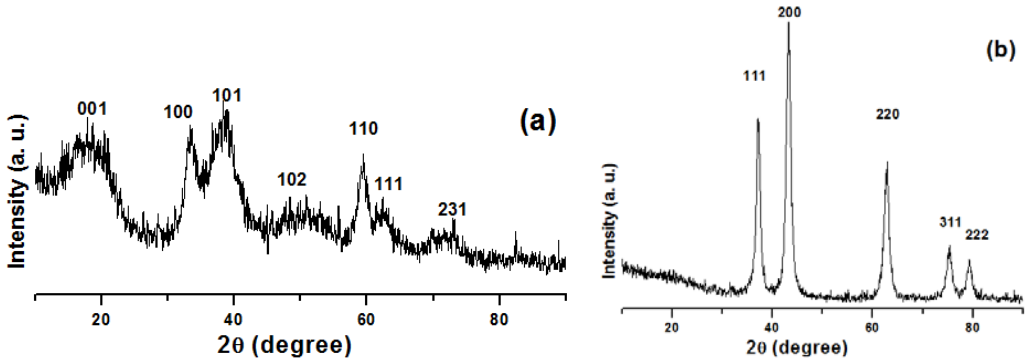

Fig. 3. XRD patterns of the prepared (a) $Ni(OH)_2$ and (b) NiO nanoparticles

All of the diffraction peaks in the hydroxide pattern (Fig. 3a) can be easily indexed to a brucitephaseof β-$Ni(OH)_2$ with cell constants of a=3.126 Å and c=4.662 Å (JCPDS 74-2075). Notably, the broadening of the peaks in Fig. 3a indicates the nanoscale dimensionality of the deposited hydroxide. In general, the broadening of XRD diffraction peaks may result from small grain sizes or structural microdistortions in crystal. As confirmed by the SEM and TEMimages (Fig. 9), the prepared nickel hydroxide has composed of ultrafine nanoparticles. So, it can be said that a significant broadening of the diffraction peaks in the XRD pattern of β-$Ni(OH)_2$ has resulted from its extremely small particle structure. Fig. 3b shows the XRD pattern of electrodeposited $Ni(OH)_2$ after annealing of at 700 ^oC for 3h. The indexed peaks in this pattern are fully consistent with the cubic NiO (JCPDS 47-1049). In addition, no peaks for any impurities i.e. $Ni(OH)_2$ or other phases were observed in the pattern which further confirm the purity of the obtained crystalline phase of NiO. The observed sharp peaks also confirmed a well-crystallized NiO powder.

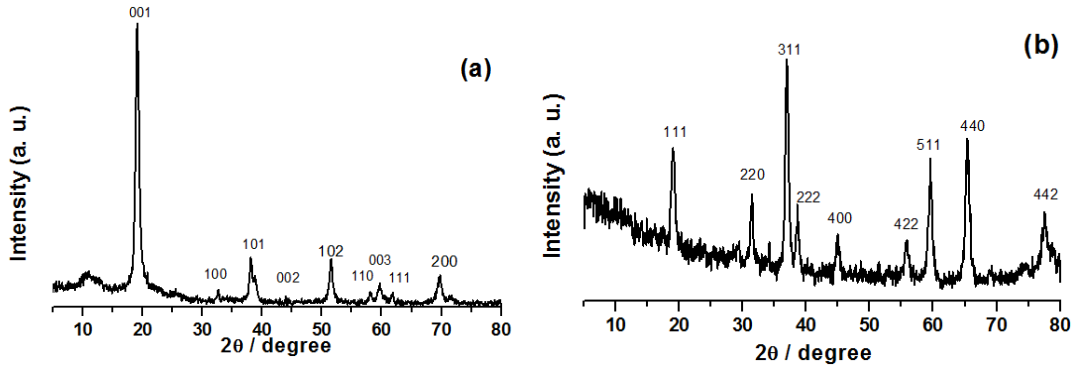

Fig. 4. XRD patterns of the prepared (a) $Co(OH)_2$ and (b) Co_3O_4 nanoparticles

The XRD patterns of the cobalt hydroxide compounds before and after heat treatment are shown in Fig. 4. All diffraction peaks of hydroxide deposit are related to the brucite-like phase of $Co(OH)_2$ (hexagonal structure, JCPDS 30–443). No diffraction peaks of α phase

were observed, indicating the high purity of the β phase has been successfully prepared under our experimental conditions. The XRD pattern of the oxide sample is shown in Fig. 4b. All diffraction peaks in this pattern can be indexed undisputedly to face-centered cubic (fcc) Co_3O_4 phase (JCPDS 43-1003). No other phases were observed, demonstrating that the deposited hydroxide was completely transformed into Co_3O_4 after heat-treatment at 700 ^oC for 3h. The XRD pattern in Fig. 5a can be assigned to $Gd(OH)_3$ which exhibits two very broad peaks near $2\theta=30^o$ and 50^o, and so is essentially amorphous [31]. Also, all diffraction peaks in Fig. 5b can be easily indexed to the cubic Gd_2O_3 phase (JCPDS 88-2165). No diffraction peaks from impurities were observed.

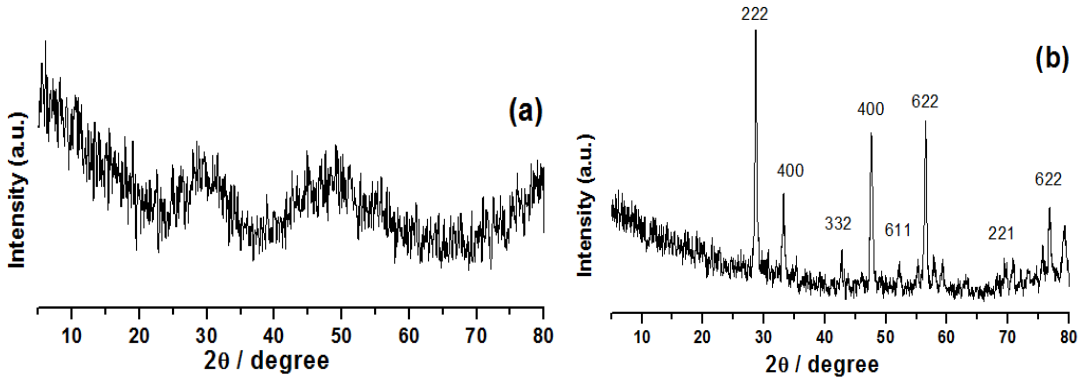

Fig. 5. XRD patterns of the prepared (a) $Gd(OH)_3$ and (b) Gd_2O_3 nanoparticles

It was reported that the nitrate ions are necessarily intercalated in their hydroxide structures [46-48]. In addition, the nitrate intercalation is highly depends on the experimental parameters and also the ions are not always insert in the growing layers. For example, characterization of thin yttrium films formed by electrogeneration of base in nitrate bath showed that the nitrate anions are intercalated in yttrium hydroxide structure [47]. Bouchaud*et al.* have also clearly demonstrated that only trapped anions were retained in the synthesized cerium hydroxides and nitrate content is highly dependent on the rinsing media after the elaboration [48].The nitrate content of our hydroxide samples were analyzed by CHN analysis and the results are listed in Table 1. The presence of nitrogen in the prepared hydroxide powders deal with to the trapped nitrate ions in their structures. The observed H and C contents are related to the structural and physically adsorbed water, and carbonate groups (originating from the reaction of the $M(OH)_n$ deposit with the CO_2 from air), respectively.

Table 1. Results of CHN and TG analyses of the prepared hydroxide samples

Sample name	CHN Results			TG results	
	N (%)	H (%)	C (%)	Physically adsorbed water (%)	Total weight loss (%)
$La(OH)_3$	1.08	2.21	0.92	3.2	14.3
$Gd(OH)_3$	2.17	3.05	0.57	12.4	37.2
$Ni(OH)_2$	2.99	2.32	0.71	11.7	30.4
$Co(OH)_2$	2.64	2.94	0.84	2.4	16.5

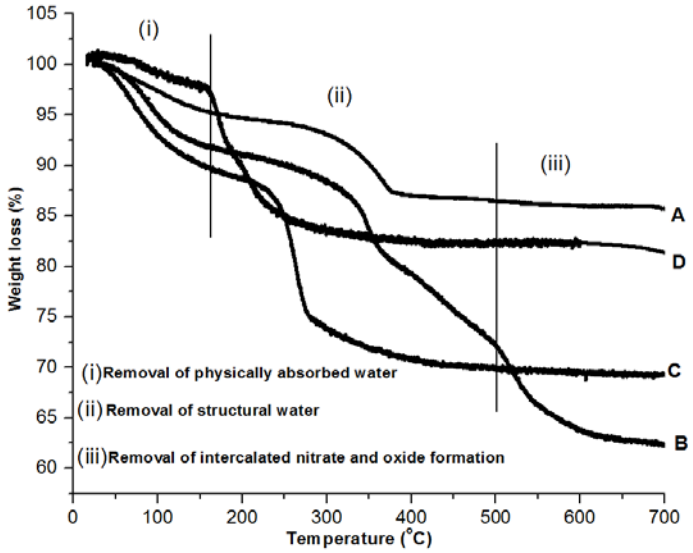

Fig. 6. TG analysis of the prepared (A) $La(OH)_3$, (B) $Gd(OH)_3$, (C) $Ni(OH)_2$ and (D) $Co(OH)_2$ nanoparticles

The thermogravimetric analysis (TGA) curves of the prepared hydroxides samples are presented in Fig. 6. It can be observed that the three distinct weight losses indicating three successive stages of physicochemical changes during the heat treatment. The first weight loss at temperature up to 150^{o}C is related to the dehydration of free and physically absorbedmolecular water associated with the prepared hydroxide deposit. The next one at temperatures between 150 and 500^{o}C, is related to the removal of the structural water. According the literature [50,51], the intercalated nitrate ions in the deposit structure are generally removed at the elevated temperatures relative to the structural water. Thus, the last weight loss can be related to the elimination of the intercalated nitrate ions from the

hydroxide structure and the formation of final oxide products. These changes are also supported by the XRD patterns (Figs. 2-5b), showing the existence of crystalline cubic phase at 700°C for La_2O_3, Gd_2O_3, NiO and Co_3O_4. The results observed from TG curves are listed in Table 1. Finally, the following sequence as a general mechanism appears to interpret the three weight loss steps related to the thermogravimetric and accompanied structural changes observed in Fig. 6:

$$[M(OH)_{(n-x)}(NO_3)_x \, .yH_2O] \rightarrow [M(OH)_{(n-x)}(NO_3)_x] + yH_2O \quad (n=2 \text{ or } 3) \tag{4}$$

$$[M(OH)_{(n-x)}\,(NO_3)_x] \rightarrow [MO(OH)_{(n-2-x)}(NO_3)_x] + H_2O \tag{5}$$

$$[MO(OH)_{(n-2-x)}\,(NO_3)_x] \rightarrow \; MO + 2xNO_2 \; + (n-2-x)H_2O + (n-2)/2\; O_2 \tag{6}$$

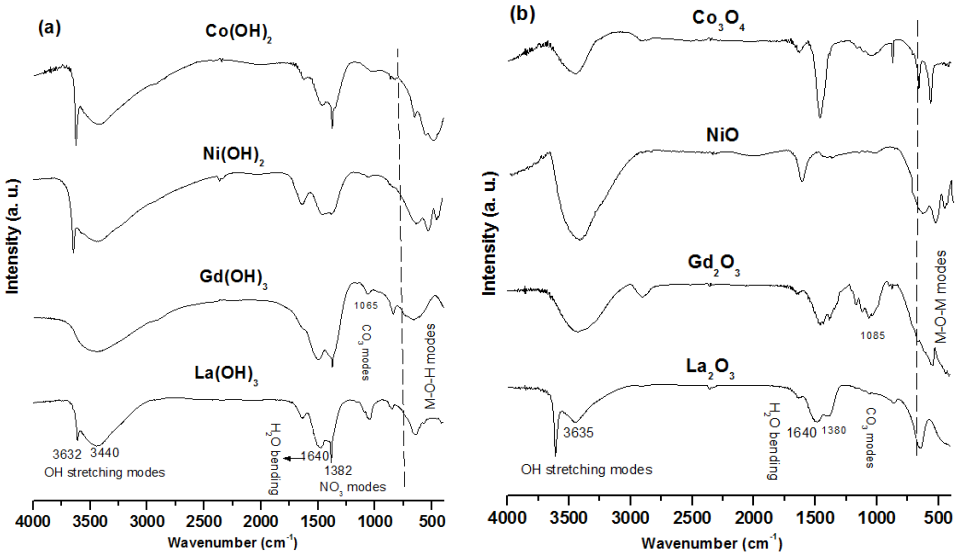

Fig. 7. IR spectra of the prepared (a) hydroxides and (b) oxides nanoparticles

Fig. 7 shows IR spectra of the prepared metal oxide and hydroxide fine particles. In all spectra, the bands at approximately 3460 and 1640 cm^{-1} are due to the (O–H) stretching vibration and (O–H) deformation vibration of the adsorbed water, respectively. As seen in Fig. 7b, the vibration intensity of OH group decreases markedly, however, they still exist in the annealed oxide samples due to moisture absorption during the testing. The peaks at about 1540 and 1085 cm^{-1} can be also attributed to the carbonate group, which may also originate from air. In Fig. 7a, the peaks at approximately 640 and 560 cm^{-1} deal with the M–O–H stretching modes. Following the calcinations of the hydroxide samples at 700°C, new bands appeared at approximately 670, 495 and 420 cm^{-1} (Fig. 7b). The bands are characteristic of metal–oxygen stretching frequency of La_2O_3, Gd_2O_3, NiO and Co_3O_4 [52].

Surface morphology and particle size of the prepared samples were determined by SEM and TEM techniques. Figs. 8-11 exhibit the morphological properties of the prepared metal

hydroxide and oxide samples. The SEM images show the particle shape morphology for all prepared hydroxide and oxide samples. However, due to the ultrafine size of the particles of the prepared samples, more information could not be detected from the SEM images. High magnification by TEM revealed that the prepared samples are composed of well–dispersed ultrafine particles with the sizes of about 10 nm. It should be noted that a rather agglomerated particle morphology is seen for $Co(OH)_2$ and Co_3O_4 in the SEM images (Fig. 11). In fact, all of the oxide and hydroxide products are composed of ultrafine particles, which are well–dispersed without agglomeration. It should be noted that the Co_3O_4 sample has undergone some agglomerations which its particle size reaches 15 nm (as can be seen from Fig. 11d).

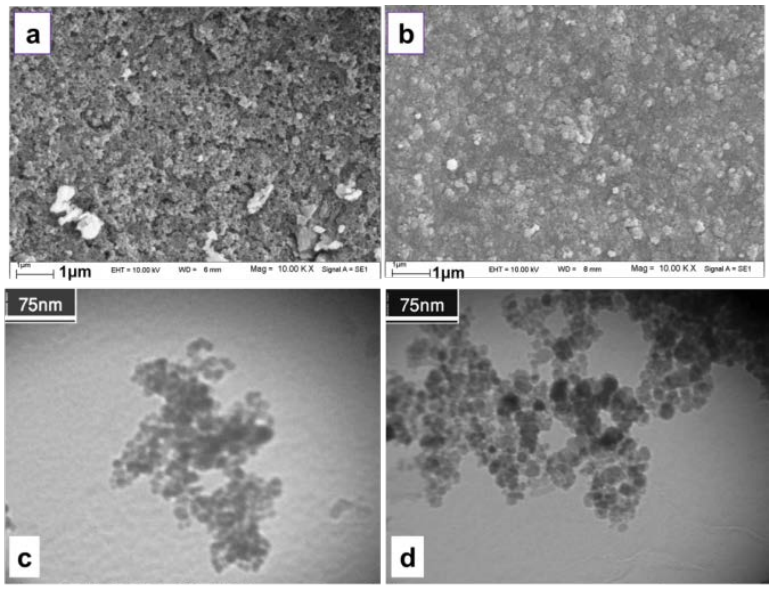

Fig. 8. SEM (a and b) and TEM (c and d) images of the prepared $La(OH)_3$ and La_2O_3 nanoparticles, respectively

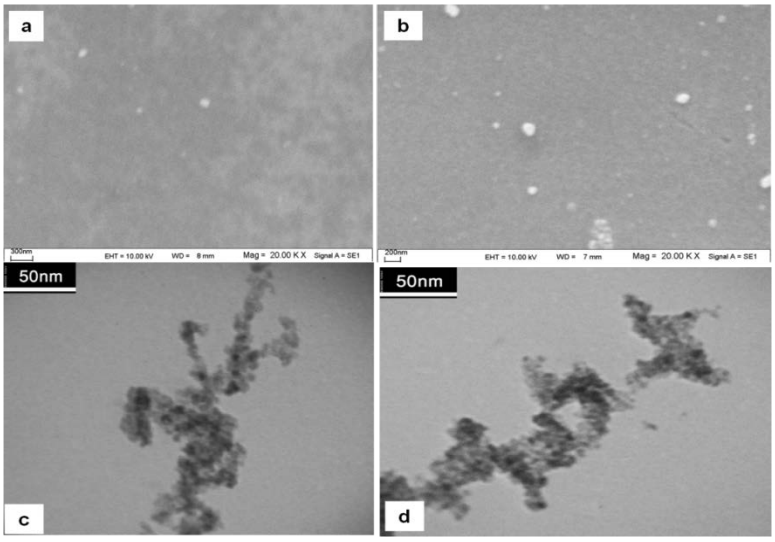

Fig. 9. SEM (a and b) and TEM (c and d) images of the prepared $Gd(OH)_3$ and Gd_2O_3 nanoparticles, respectively

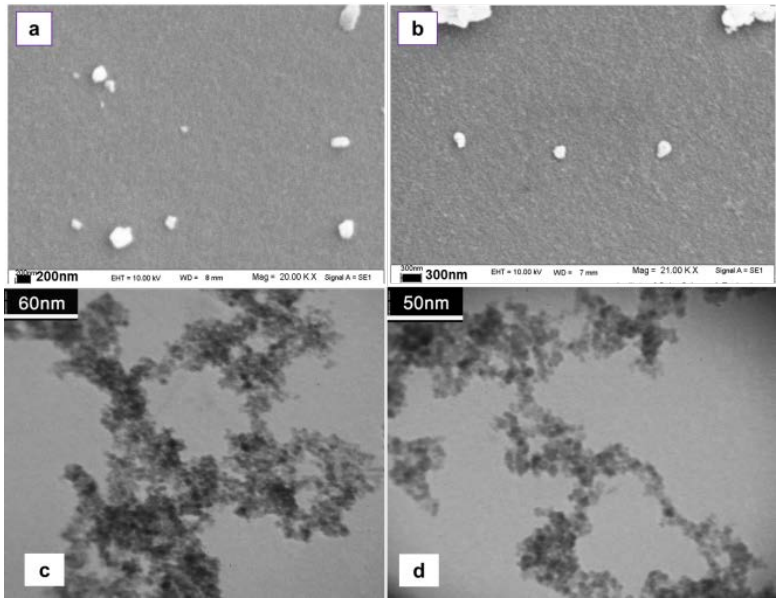

Fig. 10. SEM (a and b) and TEM (c and d) images of the prepared $Ni(OH)_2$ and NiO nanoparticles, respectively

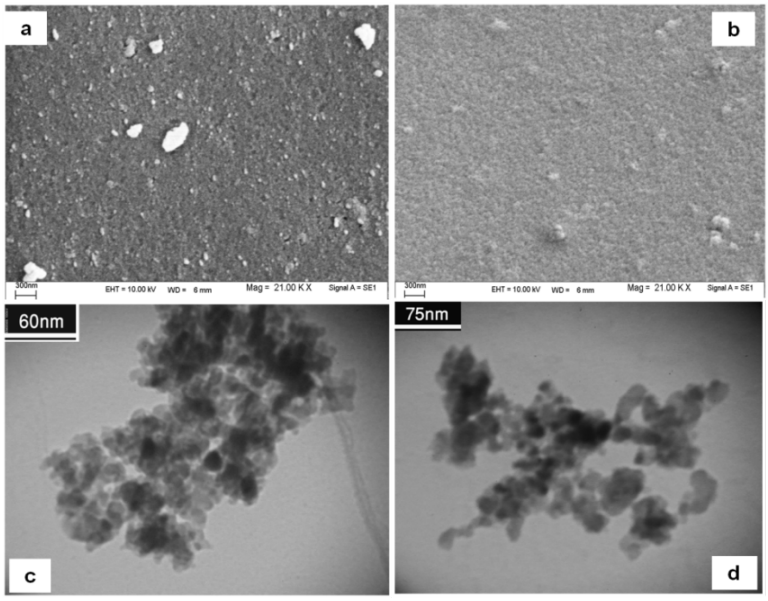

Fig. 11. SEM (a and b) and TEM (c and d) images of the prepared $Co(OH)_2$ and Co_3O_4 nanoparticles, respectively

To determine the particles size of the prepared samples, their average crystallite size (D) was calculated from the width of the XRD peaks through using the Scherrer equation ($D=0.9\lambda/\beta\cos\theta$), where, $\lambda$is the wavelength of X-ray radiation, $\theta$is the Bragg angle of the peak and β(FWHM) is defined as the full-width at half maximum of the diffraction peak in radians. The average crystallite sizes of the prepared La_2O_3, Gd_2O_3, NiO and Co_3O_4nanoparticles were estimated to be 7, 5, 6 and 11 nm.The average crystallite size of the β-$Ni(OH)_2$ nanoparticles was also calculated to be about 4 nm from the width of the (101)

peak at 2θ=39.1° (Fig. 3a) through using the Scherrer equation which is in agreement with TEM observations (Fig. 10c).These results indicated that the preparation of the metal hydroxides and oxides nanoparticles with ultrafine size is easily achievable by low-temperature cathodic electrodeposition with applying the optimum current density.

4. CONCLUSION

Ultrafine nanoparticles of $M(OH)_n$ (M=La, Gd, Ni and Co) were prepared by cathodic electrodeposition at mild conditions, i.e. low bath temperature and low applied current density. Morphological characterization showed that the prepared $M(OH)_n$ samples have smooth and uniform morphology with a particle size of about 5 nm. Heat–treatment of the prepared $M(OH)_n$ nanoparticles at 700°C led to the formation of well−dispersed ultrafine oxide nanoparticles. The average crystallite size of the prepared metal oxides particles was calculated to be around 10 nm and confirmed by TEM. Based on the findings in this work, it was concluded that low-temperature cathodic electrodeposition (at the applied current density of 1 mA cm^{-2}) followed by heat-treatment (at 700°C for 3h) can be recognized as an easy and effective route for the synthesis of metal oxide and hydroxide ultrafine nanoparticles.

REFERENCES

[1] M. S. Wu, Y. H. Ou, and Y. P. Lin, J. Electrochem. Soc. 158 (2011) A231.
[2] A. Shiralizadeh Dezfuli, M. R. Ganjali, P. Norouzi, and F. Faridbod, J. Mater. Chem. B 3 (2015) 2362.
[3] A. Shiralizadeh Dezfuli, M. R. Ganjali, H. R. Naderi, and P. Norouzi, RSC Adv. 5 (2015) 46050.
[4] E. A. Olivetti, K. C. Avery, I. Taniguchi, D. R. Sadoway, and A. M. Mayes, J. Electrochem. Soc. 155 (2008) A488.
[5] S. N. S. Goubert-Renaudin, and X. Zhu, J. Electrochem. Soc. 159 (2012) B426.
[6] M. R. Ganjali, P. Norouzi, M. Adib, and A. Ahmadalinezhad, Anal. Lett. 39 (2006) 1075.
[7] F. Wang, Z. Wang, M. Wu, X. Guo, C. Wang, and M. Zhang, J. Rare Earths 28 (2010) 139.
[8] Y. Chang, Z. Ling, Y. Li, and X. Hu, Electrochim. Acta 93 (2013) 241.
[9] L. Xiang, Y. P. Yin, and Y. Jin, Mater. Lett. 59 (2005) 2223.
[10] M. R. Ganjali, H. A. Zamani, P. Norouzi, M. Adib, and M. Rezapour, Bull. Korean Chem. Soc. 26 (2005) 579.
[11] J. Lee, and Y. Tak, J. Industrial Engin. Chem. 5 (1999) 139.
[12] I. Zhitomirsky, and A. Petric, J. Mater. Chem. 10 (2000) 1215.
[13] I. Avramova, D. Stoychev, and T. Marinova, Appl. Sur. Sci. 253 (2006) 1365.

[14] M. R. Ganjali, M. Tahami, M. Shamsipur, T. Poursaberi, S. Haghgoo, and M. Hosseini, Electroanalysis 15 (2003) 1038.
[15] M. Aghazadeh, M. Ghaemi, A. Nozad, and A. Ahmadi, Mater. Lett. 65 (2011) 2545.
[16] M. Aghazadeh, A. Nozad, H. Adelkhani, and M. Ghaemi, J. Electrochem. Soc. 157 (2010) D519.
[17] T. Yousefi, M. Aghazadeh, A. Nozad, and M. H. Mashadizadeh, Sci. Adv. Mater. 4 (2012) 214.
[18] T. Yousefi, and M. Aghazadeh, J. Nanoengin. Nanomanufact. 2 (2012) 248.
[19] M. Aghazadeh, T. Yousefi, and M. Ghaemi, J. Rare Earths 30 (2012) 281.
[20] M. Aghazadeh, T. Yousefi, and M. Ghaemi, J. Rare Earths 30 (2012) 236.
[21] L. G. Rovira , J. M. Sanchez-Amaya, M. Lopez-Haro, A. B. Hungria, Z. Boukha, S. Bernal, and F. J. Botana, Nanotechnology 19 (2008) 495305.
[22] D. Zheng, J. Shi, X. Lu, and C. Wang, Cryst. Engin. Commun. 10 (2010) 4066-4070.
[23] C. Z. Yao, B.H. Weia, H. X. Ma, Q. J. Gong, K. W. Jing, H. Sun, and L. X. Meng, Mater. Lett. 65 (2011) 490.
[24] D. Jiawen, W. Yanli, S. Weili, and L. Yongiu, J. Rare Earths 24 (2006) 440.
[25] P. Bocchetta, M. Santamaria, and F. D. Quarto, Electrochem. Commun. 9 (2007) 683.
[26] H. A. Zamani, G. Rajabzadeh, M. R. Ganjali, and S. M. Khatami, Electroanalysis 17 (2005) 2260.
[27] M. Aghazadeh, A. Nozad, M. Ghaemi, and T. Yousefi, Mater. Lett. 65 (2011) 1466.
[28] M. Aghazadeh, A. Nozad, M. Ghaemi, and T. Yousefi, J. Electrochem. Soci. 158 (2011) E136.
[29] F. Khosrow-pour, M. Aghazadeh, and B. Arhami, J. Electrochem. Soci. 160 (2013) D150.
[30] F. Khosrow-pour, M. Aghazadeh, B. Sabour, and S. Dalvand, Ceram. Int. 39 (2013) 9491.
[31] I. Zhitomirsky, and A. Petric, Mater. Lett. 42 (2000) 273.
[32] M. Aghazadeh, and T. Yousefi, Mater. Lett. 73 (2012) 176.
[33] F. Abed, M. Aghazadeh, and B. Arhami, Mater. Lett. 99 (2013) 11.
[34] D. D. Zhao,S. J.Bao, W. J. Zhou,and H. L. Li, Electrochem. Commun. 9 (2007) 869.
[35] M. R. Ganjali, H. A. Zamani, P. Norouzi, M. Adib, and M. Accedy, Acta Chim. Slov. 52 (2005) 309.
[36] M. Aghazadeh, A. Nozad, and M. Ghaemi, Int. J. Hydrogen Energy 36 (2011) 8674.
[37] H. Mohammad Shiri, and M. Aghazadeh, J. Electrochem. Soc. 159 (2012) E132.
[38] K. R. Prasad, and N. Miura, Appl. Phys. Lett. 85 (2004) 4199.
[39] J. R. S. Brownson, and C. Levy-Clement,Electrochim. Acta 54 (2009) 6637.
[40] W. J. Zhou, J. Zhang, T. Xue, D. D. Zhao, and H. L. L i,J. Mater. Chem. 18 (2008) 905.
[41] M. Shamsipur, M. Yousefi, M. Hosseini, and M. R. Ganjali, Anal. Lett. 34 (2001) 2249.

[42] M. Aghazadeh, M. Hosseinifard, B. Sabour, and S. Dalvand, Appl. Surf. Sci. 287 (2013) 187.
[43] M. Aghazadeh, A.A. Malek Barmi, and T. Yousefi, J. Iran.Chem. Soc. 9 (2012) 225.
[44] M. Aghazadeh,J. Appl. Electrochem. 42 (2012) 89.
[45] A. A. Malek Barmi, M. Aghazadeh, B. Arhami, H. Mohammad Shiri, A. Amini Fazl, and E. Jangju, Chem. Phys. Lett. 541 (2012) 65.
[46] I. Zhitomirsky, Adv. Coll. Interf. Sci. 97 (2002) 279.
[47] J. M. Brossard, J. Balmain, J. Creus, and G. Bonnet, Coatings Technol. 185 (2004) 275.
[48] B. Bouchaud, J. Balmain, G. Bonnet, and F. Pedraza, Electrochim. Acta 88 (2013) 798.
[49] Y. Hamlaoui, F. Pedraza, C. Remazeilles, S. Cohendoz, C. Rebere, L. Tifouti, and J. Creus, Mater. Chem. Phys. 113 (2009) 650.
[50] M. Karppinen, P. Kylgikoski, L. Niinist, and C. Rodellas, J. Thermal Analysis 35 (1989) 347.
[51] J. M. Haschke, Inorg. Chem. 13 (1974) 1812.
[52] R. A. Nyquist, and R. O. Kagel, Handbook of Infrared and Raman Spectra of Inorganic Compound and Organic Salts, Vol. 4, p. 223, Academic Press, Tokyo (1997).